

# Memory-Augmented Hybrid Quantum Reservoir Computing

J. Settino,<sup>1,2,3</sup> L. Salatino,<sup>3</sup> L. Mariani,<sup>3</sup> M. Channab,<sup>4</sup> L. Bozzolo,<sup>4</sup> S. Vallisa,<sup>5</sup> P. Barillà,<sup>4</sup>  
A. Policicchio,<sup>4</sup> N. Lo Gullo,<sup>1,2,3</sup> A. Giordano,<sup>3</sup> C. Mastroianni,<sup>3</sup> and F. Plastina<sup>1,2</sup>

<sup>1</sup>*Dipartimento di Fisica, Università della Calabria, Via P. Bucci Arcavacata di Rende (CS), Italy*

<sup>2</sup>*INFN, Gruppo collegato di Cosenza, Italy*

<sup>3</sup>*ICAR, Consiglio Nazionale delle Ricerche, Italy*

<sup>4</sup>*NTT Data Via Calindri, 4 Milano, Italy*

<sup>5</sup>*Fondazione ISI via Chisola 5 Torino*

(Dated: November 13, 2024)

Reservoir computing (RC) is an effective method for predicting chaotic systems by using a high-dimensional dynamic reservoir with fixed internal weights, while keeping the learning phase linear, which simplifies training and reduces computational complexity compared to fully trained recurrent neural networks (RNNs). Quantum reservoir computing (QRC) uses the exponential growth of Hilbert spaces in quantum systems, allowing for greater information processing, memory capacity, and computational power. We present a hybrid quantum-classical approach that implements memory through classical post-processing of quantum measurements, thus, avoiding the need for multiple coherent input injections (as in the original QRC proposal). We tested our model on two physical platforms: a fully connected Ising model and a Rydberg atom array, and evaluated it on various benchmark tasks, including the chaotic Mackey-Glass time series prediction, where it demonstrates significantly enhanced predictive capabilities and achieves a substantially longer prediction time, outperforming previously reported approaches.

## I. INTRODUCTION

Reservoir Computing (RC) is a computational framework that has gained significant attention for efficiently processing time-dependent data. Originally inspired by recurrent neural networks (RNNs), RC exploits the dynamics of a fixed, high-dimensional system, known as the reservoir, to transform input signals into a rich, dynamic representation [1, 2]. This transformation allows for the linear extraction of complex features, making RC particularly suitable for tasks such as time series prediction, pattern recognition, and control systems. The key advantage of RC lies in its simplicity and efficiency. Unlike traditional RNNs, where the entire network is trained, RC requires training only on the output layer, while the reservoir remains untrained [1–7]. RC systems can be implemented in quantum domains, exploiting quantum mechanics properties to further enhance computational power and memory capacity. Quantum computing offers new paradigms in information processing by utilizing principles like superposition, entanglement, and quantum interference, allowing for exponential increases in computational power and memory space. These features enable quantum systems to tackle problems that are computationally infeasible for classical systems [8–19]. The first proposal of Quantum Reservoir Computing (QRC) by Fujii and Nakajima [20] utilizes the space of quantum density matrices to store and process information, by injecting the input data into the state of one qubit of a fully connected qubit network.

Building on that foundational work, researchers have investigated a variety of platforms, each offering specific advantages for Quantum Reservoir Computing (QRC) [21–24]. Among these, spin chains have been extensively studied across a wide range of

tasks, from time series prediction to Extreme Learning Machines [25–41]. Additionally, fermionic and bosonic systems have been proposed as alternative physical implementation of reservoir [42–44]. Other explored set-ups include quantum oscillators [45, 46], photonic systems for both Quantum RC [47], and Quantum Extreme Learning Machines [48], and Rydberg atoms, which offer strong dipole-dipole interactions as a key feature [49, 50], with platforms such as Bloqade by QuEra enabling the simulation of many-body quantum systems. Furthermore, gate-based platforms have recently been explored for implementing QRC algorithms, due to their universality and high controllability [51–58].

Despite their theoretical promise, protocols based on Fujii’s approach require multiple copies of the quantum system, rendering them experimentally impractical. To address this challenge, hybrid approaches have been proposed [43, 54, 58, 59], drawing inspiration from classical reservoir computing [60–63]. In these hybrid models, quantum evolution is combined with classical post-processing, providing a more feasible solution for practical implementation. However, these hybrid systems often suffer from a significant drawback: the loss of memory concerning previous steps. Feedback mechanisms, wherein the result of the previous step is reintroduced into the system at the subsequent step, have been proposed to address this issue [33, 54, 59, 64].

In this work, we introduce a novel quantum-classical hybrid approach that integrates a simple classical post-processing component to boost memory capacity by exploiting classical memory resources, bridging between QRC and Extreme Learning Machine. We assess the performance of our algorithm across several benchmark tasks, including linear memory, NARMA, and, finally, time series prediction using the Mackey-Glass series. Our

approach is tested on two different physical systems: a fully connected Ising model in a transverse field and a system utilizing Rydberg atoms. For both of the cases, we find a substantial enhancement of predictive capabilities.

The paper is structured as follows. In Sec. II, we introduce the hybrid quantum-classical reservoir computing model and detail the methods used to enhance memory capacity through classical post-processing. Sec. III presents the implementation of our model on two distinct physical systems: a fully connected Ising model and a Rydberg atoms platform. We discuss the results of applying our approach to various benchmark tasks, including linear memory, NARMA, and Mackey-Glass time series prediction. Finally, in Sec. IV, we summarize our findings and discuss future directions for the development of quantum reservoir computing.

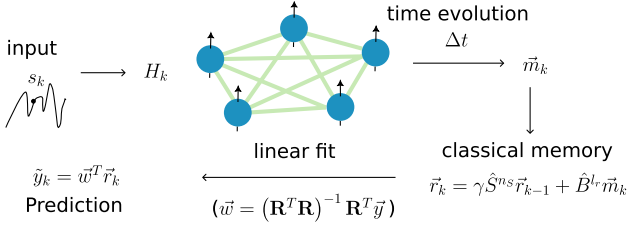


FIG. 1. Schematic representation of the proposed hybrid quantum-classical reservoir computing (QRC) method. At each step  $k$ , the input data  $\{s_k\}$  is encoded into the quantum reservoir by modulating a parameter of the Hamiltonian  $H_k$ , which generates the dynamics of a quantum system (e.g., a transverse-field Ising model or Rydberg atom array). The system evolves for a time  $\Delta t$ , giving rise to the quantum state  $|\psi_k(\Delta t)\rangle$ , depending on the input. After the time evolution, the output is obtained by measuring a set of observables  $\vec{m}_k$ , which carry information about the input data. These measurements are further processed classically to construct a reservoir state  $\vec{r}_k$  that retains the memory of previous inputs. A linear fit is then applied to the reservoir state to produce the predicted output, thereby allowing the system to solve complex tasks such as time series prediction with enhanced memory capacity.

## II. METHOD

We introduce a model of quantum reservoir computing where the input is encoded into the system by varying a Hamiltonian parameter. Our model uses a Hamiltonian similar to that proposed by Fujii and Nakajima [20]; namely, a transverse-field Ising model with an additional input-dependent magnetic field aligned with the coupling terms:

$$\hat{H}_k = \sum_{i < j} J_{ij} \hat{\sigma}_i^x \hat{\sigma}_j^x + h \sum_i \hat{\sigma}_i^z + h_k \sum_i \hat{\sigma}_i^x, \quad (1)$$

where  $J_{ij}$  represents the coupling constants,  $h$  is the

static magnetic field, and  $h_k$  is the additional magnetic field containing the information about the  $k$ -th value of the input sequence  $\{s_k\}$ . For each input  $s_k$  a target function  $y_k(\{s_{k'}\}_{k' \leq k})$  is identified, which generically depends on the previous values of the input sequence.

For each input data, a pure state  $|\psi_0\rangle$  is evolved for a time  $\Delta t$  according to the Hamiltonian  $\hat{H}_k$ ,  $|\psi_0^k(\Delta t)\rangle = e^{-i\hat{H}_k \Delta t} |\psi_0\rangle$ . After this evolution, the expectation values of a set of observables,  $\vec{m}_k$ , are measured.

Since the evolution is driven only by the current input  $s_k$ , we aim to construct a reservoir state that retains memory of previous states. Inspired by the structure of classical RNNs [60–63], we define the “reservoir state” by incorporating two additional operators ( $\hat{S}^{n_s}$  and  $\hat{B}^{l_r}$ ) into the classical framework:

$$\vec{r}_k = \gamma \hat{S}^{n_s} \vec{r}_{k-1} + \hat{B}^{l_r} \vec{m}_k. \quad (2)$$

$\hat{S}^{n_s}$  and  $\hat{B}^{l_r}$  act on the reservoir state at the previous step and the measurement vector, respectively, with  $\gamma$  being a real-valued parameter between 0 and 1 that weighs the previous input.  $\hat{S}^{n_s}$  acts on a generic vector by shifting the vector elements by  $n_s$  steps forward, if positive, or backward, if negative,  $([\hat{S}^{n_s}]_{ij} = \delta_{(i+n_s) \bmod l_r, j})$ . It coincides with a cyclic permutation of the reservoir vector and can be represented by an orthogonal matrix. Its role is to enhance the distinguishability of the inputs at different times by avoiding the same observable being summed up at different times, thus boosting classical memory. The operator  $\hat{B}^{l_r}$  acts on the measurement vector by lengthening it, interleaving zeros between the elements such that its final length is  $l_r$ , which coincides with the length of  $\vec{r}_k$ . As an example, given a vector  $\{v_1, v_2, v_3, v_4\}$ , the action of the operator  $\hat{S}^1$  coincides with  $\hat{S}^1\{v_1, v_2, v_3, v_4\} = \{v_2, v_3, v_4, v_1\}$ , while applying  $\hat{B}^8$  introduces four zeros, resulting in  $\hat{B}^8\{v_1, v_2, v_3, v_4\} = \{v_1, 0, v_2, 0, v_3, 0, v_4, 0\}$ .

In the training phase, after the reservoir is built with the measurements coming from  $N_{tr}$  values of the input sequence, a linear fit is applied. Specifically, the predicted value at step  $k$  is given by  $\hat{y}_k = \vec{w}^T \vec{r}_k$ , with the weight vector being given by:

$$\vec{w} = (\mathbf{R}^T \mathbf{R})^{-1} \mathbf{R}^T \vec{y},$$

where  $\mathbf{R}$  is the matrix of reservoir vectors,  $\mathbf{I}$  is the identity matrix, and  $\vec{y}$  is the vector of target values on the training dataset.

To simulate the Reservoir Computing algorithm, we perform exact diagonalization of  $N=5$  spins, with  $J_{ij}$  randomly generated from a uniform distribution in  $[-J, J]$ ,  $h=0.2J$ ,  $h_k=C_s s_k$ ,  $C_s = 0.2$ ,  $\gamma = 0.95$  for the memory tasks and  $\gamma = 0.6$  for the prediction task. All energies and times are presented in units of  $J$  and  $1/J$ , respectively. A table with names for the sets of observables is provided below in Tab. I.

Set Name	Observables	Length
$\vec{m}^{X1}$	$\langle \sigma_1^x \rangle$	1
$\vec{m}^1$	$\{\langle \sigma_1^x \rangle, \langle \sigma_1^y \rangle, \langle \sigma_1^z \rangle\}$	3
$\vec{m}^N$	$\bigcup_{j=1}^N \{\langle \sigma_j^x \rangle, \langle \sigma_j^y \rangle, \langle \sigma_j^z \rangle\}$	15
$\vec{m}^{XX}$	$\{\langle \sigma_i^x \rangle\}_{i=1,\dots,N} \cup \{\langle \sigma_i^x \sigma_j^x \rangle\}_{1 \leq i < j}$	15
$\vec{m}^{1-N}$	$\{\langle \sigma_1^x \rangle, \langle \sigma_1^y \rangle, \langle \sigma_1^z \rangle\} \cup \{\langle \sigma_1^\alpha \sigma_j^\alpha \rangle\}_{1 \leq j, \alpha \in \{x,y,z\}}$	15
$\vec{m}^A$	$\{\langle \sigma_i^\alpha \rangle\}_{i=1,\dots,N}^{\alpha \in \{x,y,z\}} \cup \{\langle \sigma_i^\alpha \sigma_j^\alpha \rangle\}_{i < j, \alpha \in \{x,y,z\}}$	45

TABLE I. Sets of observables used in the analysis

### III. RESULTS

In this section, we evaluate the performance of our hybrid quantum-classical reservoir computing model. We first test the short-term memory (STM) capacity, followed by the Nonlinear Auto-Regressive Moving Average (NARMA) task. We then assess the model's predictive capabilities on the chaotic Mackey-Glass time series. Lastly, we validate the generality of our approach by simulating the model on a Rydberg atom platform.

#### A. STM task

To begin the analysis of the performance of our Reservoir Computing (RC) algorithm, we examine the simplest task: assessing the system's short-term memory (STM) capabilities, which measures the reservoir's ability to store and retrieve past input sequences. In this task, the input sequence  $\{s_k\}$  is randomly generated from a uniform distribution over the interval  $[-1, 1]$ . The goal is to obtain the input value from  $\tau$  time steps earlier:  $y_k = s_{k-\tau}$ .

Performance is measured by the memory capacity (C) for each delay  $\tau$ , defined as the square of the Pearson correlation coefficient:

$$C(\tau) = \frac{\text{cov}(y_k, \hat{y}_k)^2}{\text{var}(y_k)\text{var}(\hat{y}_k)}, \quad (3)$$

where  $\hat{y}_k$  is the predicted output, “cov” denotes covariance, and “var” denotes variance.

In Fig. 2 (top), we present the memory capacity as a function of the delay  $\tau$  for different  $\Delta t$  values, for the case with the cyclic permutation operator ( $n_s=1$ ), when using the set of observables  $\vec{m}^A$ . One can notice that the memory capacity increases with decreasing  $\Delta t$ , as the simplicity of the task does not require the nonlinearity introduced by longer time evolutions. For the smallest  $\Delta t$ , the memory remains nearly perfect up to  $(\tau=45)$ , corresponding to the reservoir dimension.

As a comparison, we also display the case without the cyclic permutation operator ( $n_s = 0$ ), red line in Fig. 2, where  $\Delta t$  has been set to its best value ( $J\Delta t = 0.01$ ). It is evident that the cyclic permutation operator is crucial

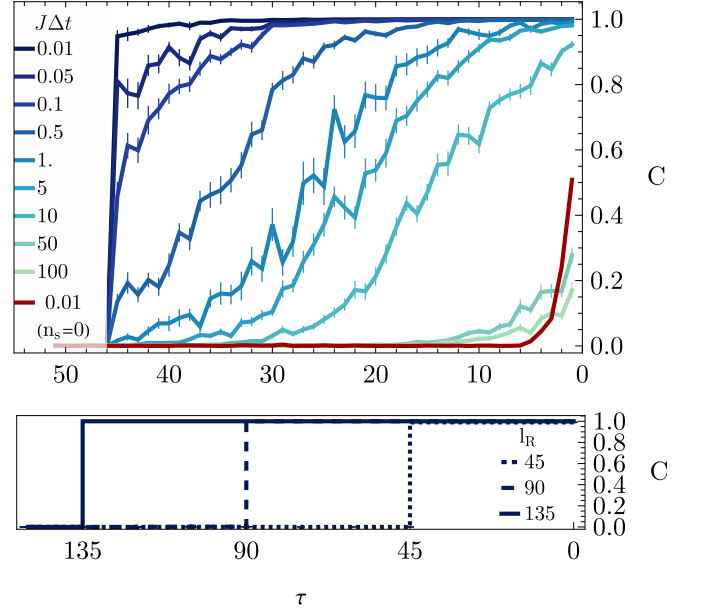


FIG. 2. Top) Memory Capacity (C) for the STM task as a function of  $\tau$  for several  $\Delta t$  values of the Hamiltonian evolution. The set of observables  $\vec{m}^A$  is used. The cyclic permutation operator is employed in all cases (with  $n_s = 1$ ), except for the red line, for which  $n_s = 0$ . Bottom) Memory Capacity as a function of  $\tau$  for several reservoir lengths  $l_r$  determined by the  $\hat{B}^{l_r}$  operator when only one observable is used ( $\vec{m}^{X1}$ ).

for retaining significant memory: the red line is almost zero for  $\tau > 2$ .

In Fig. 2 (bottom), we observe that when using the observable set  $\vec{m}^{X1}$ , which contains only one observable on a single spin, and artificially increasing the reservoir dimension through the lengthening operator  $B^{l_r}$ , it is possible to arbitrarily extend the memory capacity. This occurs because the classical memory updating function, combined with the permutation operator, allows for the storage of  $l_r$  expectation values of  $\langle \sigma_x^1 \rangle$ , which contain the injected inputs in a way that the linear fit can distinguish them.

#### B. NARMA task

To further check the performance of our RC algorithm, we test it for the Nonlinear Auto-Regressive Moving Average (NARMA) task, which is a benchmark usually employed to evaluate the non-linear memory and computational capabilities of RC systems. It involves generating a sequence where the next value depends non-linearly on both the previous ones and a random input sequence. The NARMA task with order  $n$  is defined as:

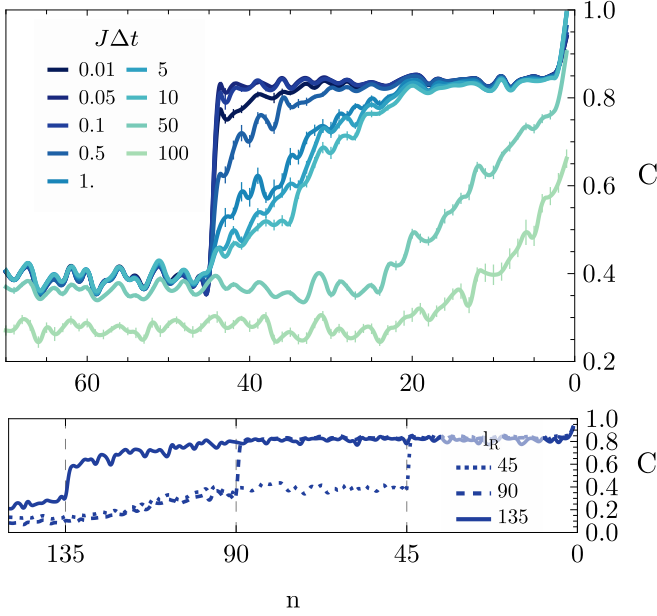


FIG. 3. Top) Pearson coefficient  $C$  for the NARMA task, as a function of the NARMA order  $n$  for several  $\Delta t$  values of the Hamiltonian evolution. The set of observables  $\vec{m}^A$  is used. Bottom)  $C$  as a function of  $n$  for several reservoir lengths  $l_r$ , determined by the  $\hat{B}^{l_r}$  operator when only one observable is used ( $\vec{m}^{X1}$ ). In both panels, the cyclic permutation operator is implemented with  $n_s = 1$ .

$$y_k = 0.3y_{k-1} + 0.05y_{k-1} \left( \sum_{i=0}^{n-1} y_{k-i-1} \right) + 1.5s_{k-n}s_{k-1} + 0.01, \quad (4)$$

where  $s_k$  is a random input uniformly distributed in the interval  $[0, 0.1]$ , and  $y_k$  is the target output. The goal is to train the reservoir system to reproduce  $y_k$  given the input sequence  $s_k$ .

The performance on the NARMA task is measured by the accuracy with which the reservoir reproduces the target output sequence; to quantify it, we use again the square of the Pearson coefficient ( $C$ ).

In Fig. 3 (top), we demonstrate that, in contrast to the linear memory task, the performance on the NARMA task does not reach its peak for the smallest  $\Delta t$ , but for  $J\Delta t \approx 0.05$ . This is because the NARMA task requires some degree of non-linearity, provided by the time evolution, to achieve optimal performance. In this case too, the non-linear memory can be significantly enhanced by increasing the reservoir dimension using the lengthening operator  $B^{n_B}$ , as illustrated in Fig. 3 (bottom).

In Fig. 4, we examine the non-linear memory capacity for the NARMA task using different sets of observables, while keeping the reservoir dimension fixed at  $l_r = 45$ . It is observed that increasing the number of observables does not lead to performance improvements. The best results,

as in the STM case, are achieved with a single observable ( $\vec{m}^{X1}$ ), which is experimentally more friendly, as it simplifies the implementation and reduces the complexity of the measurement process. This suggests that for the NARMA task, a single observable is sufficient to capture the necessary information for optimal performance. In this case, measuring more observables leads to a small decrease in performance. This is due to the fact that we fixed the reservoir dimension, so that increasing the number of observables leaves less room for classical memory.

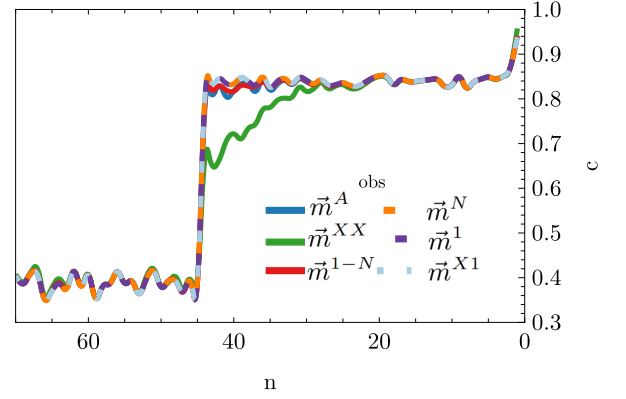


FIG. 4.  $C$  for the NARMA task as a function of the NARMA parameter  $n$  for several sets of observables (see Tab. I). Reservoir length is fixed as  $l_r = 45$ . The cyclic permutation operator is implemented with  $n_s = 1$ .

### C. Prediction task

Next, we move on to a prediction task, which is one of the primary applications of reservoir computing. This shift in focus allows us to evaluate the system's capability to forecast future values based on its internal states, which depend on the previous input data. We tested our model with the prediction of a chaotic time series, i. e. the Mackey-Glass time series. The Mackey-Glass series  $s_k$  is defined by the following delay differential equation:

$$\frac{ds(t)}{dt} = \beta \frac{s(t-\tau)}{1 + s(t-\tau)^n} - \gamma s(t) \quad (5)$$

The differential equation is numerically solved and the solution is sampled with a time step  $\delta t$ , to define the discrete sequence. Parameters are fixed as in Ref. [26]:  $\beta=0.2$ ,  $\gamma=0.1$ , delay  $\tau=17$  (chaotic behavior emerges for values greater than 17),  $\delta t=3.0$ , non-linearity parameter  $n=10$ . In the training phase, we implement a one-step forward prediction task, with  $y_k = s_{k+1}$ . In the test phase, starting from the last training time, a longer-time prediction is obtained by multiple one-step predictions.

To evaluate the performance of our reservoir model, we use the Valid Prediction Time (VPT), defined as

follows [54]. The VPT is the maximum time  $T$  for which the predicted trajectory  $\hat{y}(t)$  remains within an acceptable error margin from the true trajectory  $y(t) = s(t)$ . Mathematically, this can be expressed as:

$$VPT = \max \left\{ T : \forall t \leq T, \left( \frac{\hat{y}(t) - y(t)}{\sigma} \right)^2 < \epsilon, \right\} \quad (6)$$

where  $\epsilon = 0.3$  is a predefined error tolerance and  $\sigma$  is the standard deviation of the time series. We express VPT in integer units of the discretized time.

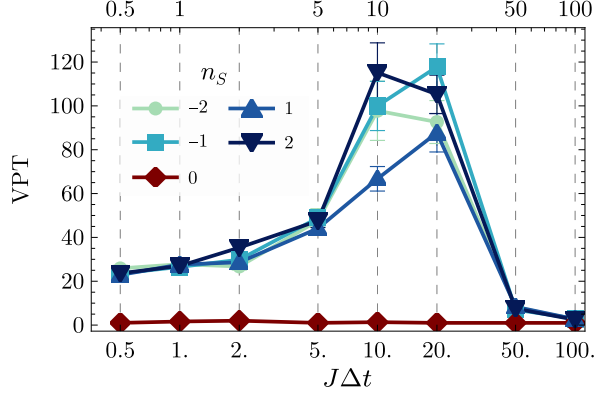


FIG. 5. VPT for the MG series prediction as a function of  $\Delta t$  in the Hamiltonian evolution for different shift numbers  $n_s$ . For each point, the mean value and standard deviation of the mean are shown, based on 30 different realizations of the Hamiltonian.

From Fig. 5, it is evident that the cyclic permutation function is crucial, as the prediction capability is negligible without it, and there are slight performance differences between various permutation functions, i.e.,  $n_s = \pm 1, \pm 2$ . The optimal evolution time for the spin network is  $J\Delta t \approx 10$ , significantly longer than the time required for memory tasks. This indicates that more complex tasks necessitate greater non-linear processing and signal distribution across the network nodes. The extended evolution time allows the system to better integrate and process the temporal dependencies inherent in the MG equation, thereby enhancing prediction accuracy.

Setting  $\Delta t$  at its optimal value, Fig. 6 (top) shows the Valid Prediction Time (VPT) as a function of the reservoir dimension, adjustable via the operator  $\hat{B}^{l_r}$ , for different sets of observables. Firstly, a general improvement in VPT is observed with increasing the reservoir dimension for all the sets of observables, up to a saturation point around 270. Using different sets of observables produces slightly varying results. Good performance is achieved with commuting observables ( $\vec{m}^{XX}$ ) or single-particle observables ( $\vec{m}^N$ ), while non-commuting and double-spin observables do not offer benefits ( $\vec{m}^{1-N}$ ). Conversely, using the biggest

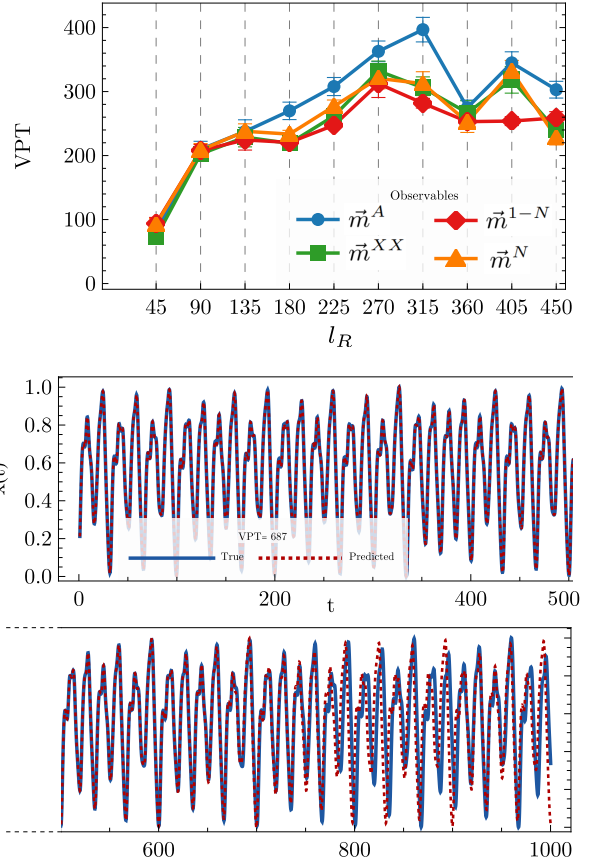


FIG. 6. Top) VPT for the MG series prediction as a function of the reservoir dimension  $l_r$  for different sets of observables. For each point, the mean value and standard deviation of the mean are shown, based on 30 different realizations of the Hamiltonian. Bottom) Example of the predicted time series for the best reservoir dimension ( $l_r = 315$ ) as a function of the integer discretized time.

considered set of observables ( $\vec{m}^A$ ) provides a slight improvement in VPT. In Fig. 6 (bottom), we present the true and predicted MG series for a specific case, with the set of observables  $\vec{m}^A$ . It is seen that the system can predict up to approximately 700 steps, which is significantly higher than recent literature results [26, 54, 59].

#### D. Simulations with Rydberg atoms

To further validate the generality of our method, we tested our algorithm on a different Hamiltonian, which is tailored to simulate the interactions in Rydberg atom arrays [49, 65]. This Hamiltonian provides a robust platform for examining the performance of quantum reservoir computing in a different physical setting, ensuring that our method is not limited to a specific type of quantum system.

The Hamiltonian in terms of spin operators is given by:

$$\begin{aligned}
H_k^R = & \sum_j \Omega_j [\sigma_j^x \cos(\varphi_{jk}) - \sigma_j^y \sin(\varphi_{jk})] \\
& - \sum_j \frac{\Delta_{jk}}{2} - \sum_j \frac{\Delta_{jk}}{2} \sigma_j^z \\
& + \sum_{j < k} V_{jk} \frac{(1 + \sigma_j^z)}{2} \frac{(1 + \sigma_k^z)}{2}.
\end{aligned} \quad (7)$$

where  $\Omega_j(t)$  is the Rabi frequency,  $\varphi_j(t)$  is the laser phase,  $\Delta_j(t)$  is the detuning and  $V_{jk}$  is the interaction term between atoms  $j$  and  $k$ . The term  $V_{jk} = \frac{C_6}{|\mathbf{x}_j - \mathbf{x}_k|^6}$  describes the van der Waals interaction, between atoms  $j$  and  $k$ . Here,  $\mathbf{x}_j$  denotes the position of the  $j$ -th atom, and the denominator  $|\mathbf{x}_j - \mathbf{x}_k|$  represents the distance between atoms  $j$  and  $k$ . The atoms are placed equally spaced with a minimum distance set to  $7\mu\text{m}$  [49]. The coefficient  $C_6$  is a constant that characterizes the strength of the interaction and depends on the specific Rydberg states being used. For our simulation, the default value of  $C_6$  is set to  $862690 \times 2\pi \text{ MHz } \mu\text{m}^6$ . This value corresponds to the interaction strength for the Rydberg state  $|r\rangle = |70S_{1/2}\rangle$  of  $^{87}\text{Rb}$  atoms. According to Ref. [49], we further set  $\Omega = 2\pi \times 4.2 \text{ MHz}$ .

Both the phases  $\varphi_j$  and the parameters  $\Delta_j$  are, in principle, capable of encoding the input information. We assessed the performance of our reservoir computing algorithm using both of these encoding methods, and the set of observables  $\vec{m}^A$ . The information about the  $k$ -th value of the input sequence  $\{s_k\}$  is encoded homogeneously, first in the value of the detuning parameter  $\Delta_{jk} = \Delta_k$ , by fixing the value of the phases to  $\varphi^*$  (Fig. 7), and subsequently in the phase  $\varphi_{jk} = \varphi_k$ , by fixing the value of  $\Delta_{jk}$  to  $\Delta^*$  (Fig. 8). In the first case, it is obtained that the maximum value of the  $VPT_{\text{Mean}}$  occurs when the influence of the spin component along the  $x$ -axis is nullified, and the component along the  $y$ -axis is maximized, thereby optimizing the interaction of the system with the external electromagnetic field. Suboptimal values are obtained for phases near  $3\pi/4$ . In the second case, the dependence on the hyper-parameter  $\Delta^*$  is more critical, the best performance is peaked at  $\Delta^* = 5\Omega$  for a specific evolution time  $\Delta t = 2$ .

The results obtained from this validation indicate that our approach retains its efficacy across different quantum systems, including those involving Rydberg atoms. The adopted Hamiltonian captures the essential features of Rydberg atom dynamics, such as the strong dipole-dipole interactions and long coherence times, which are critical for quantum information processing. Our findings suggest that the combination of classical operators for memory enhancement with the inherent quantum dynamics of Rydberg atoms can significantly improve the performance of quantum reservoir computing systems.

These results highlight the versatility of our method, demonstrating its potential applicability to a wide range of quantum systems and confirming its robustness in

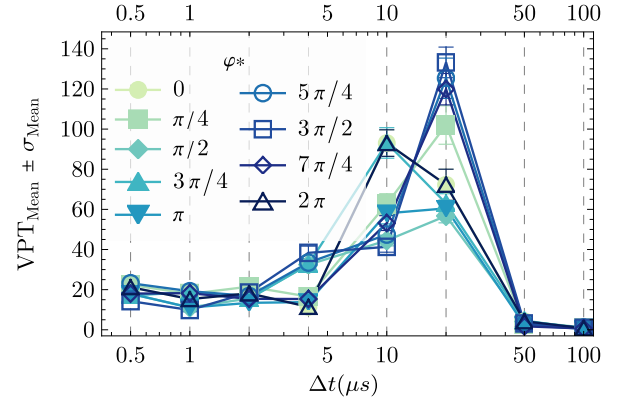


FIG. 7. VPT for the MG series prediction as a function of  $\Delta t$  of the Rydberg-atoms Hamiltonian for different values of the phases  $\varphi^*$ . The signal is encoded homogeneously in the value of the detuning parameter  $\Delta_{jk} = \Delta_k$ . For each point, the mean value and standard deviation of the mean are shown, based on 30 different realizations of the Hamiltonian.

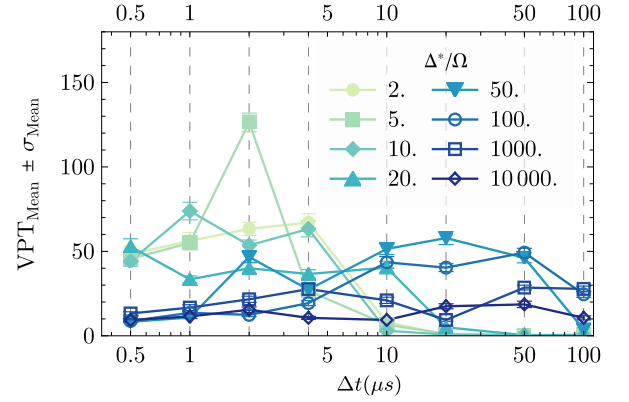


FIG. 8. VPT for the MG series prediction as a function of  $\Delta t$  of the Rydberg-atoms Hamiltonian for different values of the detuning parameter  $\Delta^*$ . The signal is encoded homogeneously in the value of the phase  $\varphi_{jk} = \varphi_k$ . For each point, the mean value and standard deviation of the mean are shown, based on 30 different realizations of the Hamiltonian.

handling different quantum Hamiltonians.

#### IV. CONCLUSIONS

In this work, we have developed a hybrid quantum-classical reservoir computing model that effectively combines the quantum dynamics of a system with classical post-processing techniques to enhance memory capacity. Our approach was designed to mitigate the challenges associated with purely quantum reservoir computing, such as requiring multiple copies of the quantum system.

We demonstrated the efficiency of our model by applying it to two distinct physical systems: a fully connected Ising model in a transverse field and a Rydberg

atom array. Both platforms showcased the versatility of our method, as they were able to successfully process information in a variety of benchmark tasks, including linear memory, NARMA, and the prediction of the chaotic Mackey-Glass time series. In particular, the Valid Prediction Time (VPT) obtained from our model outperformed several standard approaches reported in the literature, demonstrating the advanced predictive capabilities of our quantum-classical hybrid method.

The key innovation of our approach lies in the introduction of two operators in the classical post-processing phase, allowing us to extend arbitrarily the classical system's memory while maintaining the benefits of quantum information processing. The proposed method allows a continuous transition from an Extreme Learning Machine when  $\gamma = 0$  to QRC with a tunable memory via the parameter  $\gamma$ . This tunability enables optimizing the system's memory capacity according to the specific requirements of the target applications. This hybrid approach provides a promising pathway for future reservoir computing applications, particularly in cases where quantum resources are limited or expensive to replicate experimentally.

## V. ACKNOWLEDGEMENTS

JS acknowledges the contribution from PRIN (Progetti di Rilevante Interesse Nazionale) TURBIMECS - Turbulence in Mediterranean cyclonic events, grant n. 2022S3RSCT CUP H53D23001630006, CUP Master B53D23007500006, CM from ICSC - Italian Research Center on High Performance Computing, Big Data and Quantum Computing, funded by European Union - NextGenerationEU, PUN: B93C22000620006.

## Appendix A: Rydberg Hamiltonian

In the analog mode, Bloqade simulates the time evolution of a quantum state under the Schrödinger equation where the Hamiltonian is the interacting Rydberg Hamiltonian  $H$

$$i\hbar \frac{\partial}{\partial t} |\psi\rangle = H(t) |\psi\rangle \quad (\text{A1})$$

with the Hamiltonian given by:

$$\begin{aligned} \frac{H(t)}{\hbar} = & \sum_j \frac{\Omega_j(t)}{2} \left( e^{i\phi_j(t)} |0_j\rangle\langle 1_j| + e^{-i\phi_j(t)} |1_j\rangle\langle 0_j| \right) \\ & - \sum_j \Delta_j(t) \hat{n}_j + \sum_{j < k} V_{jk} \hat{n}_j \hat{n}_k \end{aligned} \quad (\text{A2})$$

where  $\Omega_j(t)$  is the Rabi frequency,  $\phi_j(t)$  is the laser phase,  $\Delta_j(t)$  is the detuning,  $\hat{n}_j = |1_j\rangle\langle 1_j|$  is the number operator and  $V_{jk}$  is the interaction term between atoms  $j$  and  $k$ .

Rewriting Eq. A2 in terms of the spin operators, we have

$$\begin{aligned} \frac{H(t)}{\hbar} = & \sum_j \Omega_j(t) \left[ \sigma_j^x \cos(\phi_j(t)) - \sigma_j^y \sin(\phi_j(t)) \right] \\ & - \sum_j \frac{\Delta_j(t)}{2} - \sum_j \frac{\Delta_j(t)}{2} \sigma_j^z \\ & + \sum_{j < k} V_{jk} \frac{(1 + \sigma_j^z)}{2} \frac{(1 + \sigma_k^z)}{2} \end{aligned} \quad (\text{A3})$$

- 
- [1] W. Maass, T. Natschl ger, and H. Markram, *Neural Computation* **14**, 2531 (2002).
  - [2] H. Jaeger and H. Haas, *Science* **304**, 78 (2004).
  - [3] D. J. Gauthier, E. Bollt, A. Griffith, and W. A. S. Barbosa, *Nature Communications* **12**, 5564 (2021).
  - [4] G. Milano, A. Cultrera, L. Boarino, L. Callegaro, and C. Ricciardi, *Nature Communications* **14**, 5723 (2023).
  - [5] G. Milano, K. Montano, and C. Ricciardi, *Journal of Physics D: Applied Physics* **56**, 084005 (2023).
  - [6] R. Ma, Q. Dai, H. Li, and J. Yang, *Chaos, Solitons & Fractals* **172**, 113523 (2023).
  - [7] R. Xiao, L.-W. Kong, Z.-K. Sun, and Y.-C. Lai, *Physical Review E* **104**, 014205 (2021).
  - [8] P. Shor, in *Proceedings 35th Annual Symposium on Foundations of Computer Science* (1994) pp. 124–134.
  - [9] L. K. Grover, in *Proceedings of the Twenty-Eighth Annual ACM Symposium on Theory of Computing*, STOC '96 (Association for Computing Machinery, New York, NY, USA, 1996) p. 212–219.
  - [10] M. A. Nielsen and I. L. Chuang, *Quantum Computation and Quantum Information: 10th Anniversary Edition* (Cambridge University Press, 2010).
  - [11] A. Montanaro, *npj Quantum Information* **2**, 1 (2016).
  - [12] J. Preskill, *Quantum* **2**, 79 (2018).
  - [13] C. Mastroianni, L. Scarcello, and J. Settino, in *2022 IEEE Intl Conf on Dependable, Autonomic and Secure Computing, Intl Conf on Pervasive Intelligence and Computing, Intl Conf on Cloud and Big Data Computing, Intl Conf on Cyber Science and Technology Congress (DASC/PiCom/CBDCoM/CyberSciTech)* (IEEE, 2022) pp. 1–7.
  - [14] C. Mastroianni, F. Plastina, L. Scarcello, J. Settino, and A. Vinci, *IEEE Transactions on Smart Grid* **15**, 444 (2023).
  - [15] C. Mastroianni, F. Plastina, L. Scarcello, J. Settino, and A. Vinci, *Numerical Computations: Theory and Algorithms NUMTA 2023*, 148 (2023).
  - [16] C. Mastroianni, F. Plastina, J. Settino, and A. Vinci, *IEEE Transactions on Quantum Engineering* **5**, 1 (2024).
  - [17] M. Consiglio, J. Settino, A. Giordano, C. Mastroianni, F. Plastina, S. Lorenzo, S. Maniscalco, J. Goold, and T. J. Apollaro, *Physical Review A* **110**, 012445 (2024).
  - [18] A. De Lorenzis, M. Casado, M. Estarellas, N. L. Gullo, T. Lux, F. Plastina, A. Riera, and J. Settino, arXiv

- preprint arXiv:2409.00998 (2024).
- [19] M. Boneberg, F. Carollo, and I. Lesanovsky, *New Journal of Physics* **25**, 093020 (2023).
  - [20] K. Fujii and K. Nakajima, *Physical Review Applied* **8**, 024030 (2017).
  - [21] P. Mujal, R. Martínez-Peña, J. Nokkala, J. García-Bení, G. L. Giorgi, M. C. Soriano, and R. Zambrini, *Advanced Quantum Technologies* **4**, 2100027 (2021).
  - [22] S. Ghosh, K. Nakajima, T. Krisnanda, K. Fujii, and T. C. Liew, *Advanced Quantum Technologies* **4**, 2100053 (2021).
  - [23] A. H. Abbas, H. Abdel-Ghani, and I. S. Maksymov, *Dynamics* **4**, 643 (2024).
  - [24] C. Zhu, P. J. Ehlers, H. I. Nurdin, and D. Soh, *ArXiv* (2024), arXiv:2405.04799 [quant-ph].
  - [25] P. Mujal, *Condensed Matter* **7**, 17 (2022).
  - [26] A. Sannia, R. Martínez-Peña, M. C. Soriano, G. L. Giorgi, and R. Zambrini, *Quantum* **8**, 1291 (2024).
  - [27] S. Mifune, T. Kanao, and T. Tanamoto, *Arxiv* (2024), arXiv:2410.07481v1.
  - [28] W. Xia, J. Zou, X. Qiu, and X. Li, *Frontiers of Physics* **17**, 1 (2022).
  - [29] W. Xia, J. Zou, X. Qiu, F. Chen, B. Zhu, C. Li, D.-L. Deng, and X. Li, *Science Bulletin* **68**, 2321 (2023).
  - [30] R. Martínez-Peña, G. L. Giorgi, J. Nokkala, M. C. Soriano, and R. Zambrini, *Physical Review Letters* **127**, 100502 (2021).
  - [31] R. Martínez-Peña, J. Nokkala, G. L. Giorgi, R. Zambrini, and M. C. Soriano, *Cognitive Computation* **15**, 1440 (2023).
  - [32] N. Götting, F. Lohof, and C. Gies, *Phys. Rev. A* **108**, 052427 (2023).
  - [33] S. Kobayashi, Q. H. Tran, and K. Nakajima, *Phys. Rev. E* **110**, 024207 (2024).
  - [34] L. Innocenti, S. Lorenzo, I. Palmisano, A. Ferraro, M. Paternostro, and G. M. Palma, *Communications Physics* **2023** 6:1 **6**, 1 (2023).
  - [35] G. L. Monaco, M. Bertini, S. Lorenzo, and G. M. Palma, *Machine Learning: Science and Technology* **5**, 035014 (2024).
  - [36] M. Vetrano, G. L. Monaco, L. Innocenti, S. Lorenzo, and G. M. Palma, *Arxiv* (2024), arXiv:2409.06782v1.
  - [37] A. Palacios, R. Martínez-Peña, M. C. Soriano, G. L. Giorgi, and R. Zambrini, *Arxiv* (2024), arXiv:2409.17734v1.
  - [38] S. Kobayashi, Q. H. Tran, and K. Nakajima, *Arxiv* (2024), arXiv:2409.12693v2.
  - [39] F. Monzani, E. Ricci, L. Nigro, and E. Prati, *Arxiv* (2024), arXiv:2409.07886v1.
  - [40] M. N. Ivaki, A. Lazarides, and T. Ala-Nissila, *ArXiv* (2024), arXiv:2409.03665 [quant-ph].
  - [41] O. Ahmed, F. Tennie, and L. Magri, *Arxiv* (2024), arXiv:2409.01394 [quant-ph].
  - [42] S. Ghosh, A. Opala, M. Matuszewski, T. Paterek, and T. C. H. Liew, *npj Quantum Information* **5**, 35 (2019).
  - [43] Q. H. Tran, S. Ghosh, and K. Nakajima, *Physical Review Research* **5**, 43127 (2023).
  - [44] G. Llodrà, C. Charalambous, G. L. Giorgi, and R. Zambrini, *Advanced Quantum Technologies* **6**, 2200100 (2023).
  - [45] L. C. Govia, G. J. Ribeill, G. E. Rowlands, H. K. Krovi, and T. A. Ohki, *Physical Review Research* **3**, 013077 (2021).
  - [46] J. Dudas, B. Carles, E. Plouet, F. A. Mizrahi, J. Grollier, and D. Marković, *npj Quantum Information* **2023** 9:1 **9**, 1 (2023).
  - [47] G. L. Giorgi, J. García-Bení, M. C. Soriano, and R. Zambrini, *Optics Express*, Vol. 32, Issue 4, pp. 6733-6747 **32**, 6733 (2024).
  - [48] A. Suprano, D. Zia, L. Innocenti, S. Lorenzo, V. Cimini, T. Giordani, I. Palmisano, E. Polino, N. Spagnolo, F. Sciarrino, G. M. Palma, A. Ferraro, and M. Paternostro, *Phys. Rev. Lett.* **132**, 160802 (2024).
  - [49] R. A. Bravo, K. Najafi, X. Gao, and S. F. Yelin, *PRX Quantum* **3**, 030325 (2022).
  - [50] M. Kornjača, H. Y. Hu, C. Zhao, J. Wurtz, P. Weinberg, M. Hamdan, ..., and S. T. Wang, *arXiv preprint arXiv:2407.02553*. (2024).
  - [51] L. Domingo, G. Carlo, and F. Borondo, *Scientific Reports* **2023** 13:1 **13**, 1 (2023).
  - [52] L. Domingo, M. Grande, G. Carlo, F. Borondo, and J. Borondo, *ArXiv* (2023), arXiv:2401.03347 [quant-ph].
  - [53] T. Yasuda, Y. Suzuki, T. Kubota, K. Nakajima, Q. Gao, W. Zhang, S. Shimono, H. I. Nurdin, and N. Yamamoto, *ArXiv* (2023), arXiv:2310.06706 [quant-ph].
  - [54] F. Wudarski, D. O'Connor, S. Geaney, A. A. Asanjan, M. Wilson, E. Strbac, P. A. Lott, and D. Venturelli, *ArXiv* (2024), arXiv:2311.14105 [quant-ph].
  - [55] D. Fry, A. Deshmukh, S. Y.-C. Chen, V. Rastunkov, and V. Markov, *Scientific Reports* **13**, 10.1038/s41598-023-45015-4 (2023).
  - [56] T. Kubota, Y. Suzuki, S. Kobayashi, Q. H. Tran, N. Yamamoto, and K. Nakajima, *Physical Review Research* **5**, 023057 (2023).
  - [57] F. G. Fuchs, A. J. Stasik, S. Miao, O. T. Kulseng, and R. P. Bassa, *ArXiv* (2024), arXiv:2407.00445 [quant-ph].
  - [58] K. Kobayashi, K. Fujii, and N. Yamamoto, *ArXiv* (2024), arXiv:2406.15783 [quant-ph].
  - [59] O. Ahmed, F. Tennie, and L. Magri, *Phys. Rev. Res.* **6**, 043082 (2024).
  - [60] G. Tanaka, T. Yamane, J. B. Héroux, R. Nakane, N. Kanazawa, S. Takeda, H. Numata, D. Nakano, and A. Hirose, *Neural Networks* **115**, 100 (2019).
  - [61] K. Nakajima, *Japanese Journal of Applied Physics* **59**, 060501 (2020).
  - [62] M. Cucchi, S. Abreu, G. Ciccone, D. Brunner, and H. Kleemann, *Neuromorphic Computing and Engineering* **2**, 032002 (2022).
  - [63] J. A. Platt, S. G. Penny, T. A. Smith, T.-C. Chen, and H. D. Abarbanel, *Neural Networks* **153**, 530 (2022).
  - [64] J. Nokkala, G. L. Giorgi, and R. Zambrini, *Machine Learning: Science and Technology* **5**, 10.1088/2632-2153/ad5f12 (2024).
  - [65] L. Henriët, L. Beguin, A. Signoles, T. Lahaye, A. Browaeys, G.-O. Reymond, and C. Jurczak, *Quantum* **4**, 327 (2020).